

Fatigue Behavior and Associated Binder Deformation Mechanisms in WC-Co Cemented Carbides

Valle V.*; Tarragó J.M. **; Llanes L. **

*Escuela Politécnica Nacional, Facultad de Ingeniería Química y Agroindustria
Quito, Ecuador (e-mail: vladimir.valle@epn.edu.ec)

** Universitat Politècnica de Catalunya, Departament de Ciència del Materials i Enginyeria Metal·lúrgica, ETSEIB
Barcelona, Spain

Resumen: La integridad mecánica de carburos cementados WC-Co ha sido estudiada por medio del análisis del crecimiento subcrítico de grietas y de la resistencia a la degradación por cargas cíclicas. La investigación se llevó a cabo en tres grados de metales duros con diferente contenido de aglutinante y/o tamaño de grano, mediante el análisis del crecimiento de grietas por fatiga y ensayos de resistencia a la fatiga a temperatura ambiente. Los resultados de resistencia a fatiga fueron comparados con datos experimentales de tenacidad de fractura y resistencia a la flexión. Bajo cargas cíclicas y dentro del contexto de la mecánica de la fatiga se puede determinar el umbral de propagación de grietas por fatiga como la tenacidad de fractura efectiva. Adicionalmente, se encontró que la aglomeración de granos gruesos y granos anormalmente gruesos constituyen los defectos críticos presentes en estos tipos de metal duro. Los resultados de EBSD sugieren que la transformación martensítica de la fase de cobalto (de fcc a hcp) no está asociada exclusivamente a la carga cíclica aplicada, sino que probablemente puede ser inducida por procedimientos de desbaste de las superficies expuestas. Desde la perspectiva de los micromecanismos de fatiga, dicha deformación se encuentra claramente localizada dentro de la fase aglutinante.

Palabras clave: Crecimiento de grietas por fatiga, Límite de fatiga, Carburos cementados.

Abstract: The mechanical integrity of WC-Co hardmetals has been studied by the occurrence of subcritical crack growth and strength degradation under cycling loading. The investigation is conducted on three WC-Co hardmetals grades with different binder content and/or grain size by assessing fatigue crack growth (FCG) behavior and fatigue life tests at room temperature. Experimental fatigue results are compared to fracture toughness and flexural strength data. An analysis of the results within a fatigue mechanics context permits to corroborate FCG threshold as the effective fracture toughness under cyclic loading. Critical defects are evidenced to be agglomerates of coarse grains and abnormally coarse grains. EBSD mapping on stable propagated cracks has been accomplished to characterize the crack-microstructure interactions within the cobalt phase. EBSD results suggest that martensitic transformation of cobalt phase (from fcc to hcp) is not exclusively associated with cyclic loading, as it had been postulated in the literature. On the other hand, it seems to be induced by rough grinding of the exposed surfaces. From the perspective of fatigue micromechanisms, they are clearly localized within the binder phase.

Keywords: Fatigue crack growth, Fatigue limit, Cemented carbides.

1. INTRODUCCION

Hard materials are generally subjected to complex combinations of stress states and environmental conditions; therefore, fracture and fatigue analysis has been considered important features in lifetime and reliability characterization [10]. Within this context, fracture of cemented carbides has been rationalized through the Linear Elastic Fracture Mechanics (LEFM). Extensive literature specifies that materials design optimization may be accomplished by the

means of fracture mechanics approach, taking into account the interaction of applied stress, fracture toughness and flaw size. Furthermore, several studies have permitted to understand that fracture process, from a microstructural view, is commonly associated with position, orientation, size and nature of the defects in materials. Hence, the presence of these parameters within material turns into propagation of cracks in an either stable or unstable mode [2]. In the case of cemented carbides aspects such as size, nature, and interaction of the phases are additional parameters to consider in the fracture process. Particularly, binder phase region in WC-Co hardmetals, despite of its relatively small size, is the responsible for providing high toughness values to the

composite material. Thus, the cobalt mean free path, and the constraint imposed by surrounding carbides grains, are generally considered important factors affecting the strength and ductility of the binder phase [8].

Extensive information shows that unstable fracture in WC-Co cemented carbide is characterized by local plasticity in the cobalt-rich binder phase, which is known as “dimples” and “ridges” due to their distinctive geometry [9]. Such features result from plastic deformation that the predominantly face center cubic cobalt (Co-fcc) undergoes during fracture. Hong and Gurland [5] observed that the required energy for propagation of the intergranular or transgranular cleavage cracks in tungsten carbides (WC) is considered to be greatly smaller than the energy necessary by the plastic deformation and ductile rupture of the binder. Consequently, it means that the plastic deformation of the binder contributes the major energy consumption process during crack propagation for cemented carbides.

On the other hand, under cyclic loads it has been evidenced that fatigue fracture surfaces of WC-Co exhibit different microstructural aspect/features as compared to those seen in unstable fracture surfaces [3]. Moreover, stress and strain fluctuations during fatigue induce to different deformation mechanisms in these materials. Then, phase transformation of cobalt binder phase has been postulated to occur as a consequence of high stresses during cycling loads and/or high accumulated deformations. According to Erling et al. [3], stable fracture in hardmetal surfaces present “step-like” features due to combination of cleavage microcracks. In this case, cracks appear to follow crystallographic planes within a length scale given by the binder mean free path [3].

During fatigue crack growth, plastic deformation of cobalt binder has been observed ahead of the crack tip. It has been found that this deformation may be limited by boundaries between cobalt grains, and at the same time, that accumulated deformation may affect the progress and path taken by subcritical crack growth. Taking into account this argument, there is a direct relationship between WC-Co hardmetals fatigue sensitivity and binder thickness [10]. Additionally, there is a substantial decrease of the crack tip shielding effect owing to reduction in ductility of the ligaments behind the crack tip leading to a reduced in fatigue resistance of hardmetals [11].

Regarding fatigue crack growth (FCG) kinetics, rates for hardmetals usually show strong dependence on maximum stress intensity factor (K_{max}). Furthermore, K_{max} values for fatigue process are considerably lower than those of fracture toughness [7]. Even though it is known that mechanical properties of these alloys are critically dependent on the physical metallurgy of binder phase region, at the present time there are few studies dealing with deformation mechanisms of the binder phase in WC-Co hardmetals during fatigue process. Indeed, literature related to allotropic

transformation of cobalt-rich phase as well as their crystallographic changes is limited [8].

2. EXPERIMENTAL PROCEDURE

2.1 Materials

The hardmetals used in this investigation were three WC-Co commercial grades namely, CoMM, CoMC and CoHM. They were supplied by Sandvik Hard Materials Company as prismatic bars of rectangular shapes with the following dimensions: 45 mm × 10 mm × 5 mm and 45 mm × 4 mm × 3 mm. Chemical composition of these samples was determined by Energy Dispersive X-ray Spectroscopy (EDS) in previous studies. Corresponding data are provided in Table 1.

Table 1: Generic microstructure and chemical composition of studied materials

| Grade | Binder Content | Grain size | Element content (wt. %) | | | |
|-------|----------------|------------|-------------------------|------|------|------|
| | | | W | Co | C | Cr |
| CoMM | Medium | Medium | 83.2 | 10.9 | 5.44 | 0.36 |
| CoMC | Medium | Coarse | 83.9 | 10.6 | 5.48 | - |
| CoHM | High | Medium | 76.5 | 18.6 | 5.00 | - |

In the same way, microstructural characterization and mechanical properties were evaluated previously. Experimental values are presented in Tables 2 and 3.

Table 2: Microstructural characteristics of the hardmetal grades investigated

| Grade | Binder content (wt. %) | Mean grain size (µm) | Contiguity | Mean free path (µm) |
|-------|------------------------|----------------------|-------------|---------------------|
| CoMM | 11.4 ± 0.44 | 1.12 ± 0.71 | 0.39 ± 0.05 | 0.44 ± 0.28 |
| CoMC | 10.6 ± 0.10 | 2.45 ± 1.37 | 0.37 ± 0.03 | 0.82 ± 0.46 |
| CoHM | 18.6 ± 0.48 | 1.15 ± 0.92 | 0.38 ± 0.05 | 0.77 ± 0.63 |

Table 3: Microstructural characteristics of the hardmetal grades investigated

| Grade | Hardness, HV30 (GPa) | Young modulus (GPa) | Weibull stress, (MPa) | Weibull modulus, m | SEPNB Fracture toughness, (MPa m ^{1/2}) |
|-------|----------------------|---------------------|-----------------------|--------------------|---|
| CoMM | 12.8 ± 0.1 | 582 ± 1 | 3149 | 36 | 14.2 ± 0.2 |
| CoMC | 11.4 ± 0.2 | 595 ± 1 | 2522 | 35 | 17.6 ± 0.6 |
| CoHM | 10.5* | 537 ± 1 | 2926 | 44 | 16.6 ± 0.6 |

*variability associated with this value was lower than 0.1

2.2 Assessment of fatigue behavior

2.2.1 Sample preparation

Fatigue crack growth threshold (K_{th}) was evaluated for the three grades using single edge notched beam rectangular samples of dimensions 45 mm × 10 mm × 5 mm. In doing so, a 3 mm depth notch was introduced by means of electron discharge machining (EDM) in six samples per grade. After that, notch tip radius was reduced by sharpening the notch

root with a blade impregnated with diamond paste. V-notches were made with tip diameter between 15 μm – 25 μm .

2.1.2 Fatigue crack growth development

The fatigue crack growth process was accomplished in a resonant testing machine with sinusoidal alternating bending loads at room temperature. Testing was conducted under four-point bending with inner and outer spans of 20 and 40 mm respectively. The crack growth was recorded by optical microscopy in a confocal scanning laser microscope Olympus OLS3100/OL3000. Crack length was assessed by removing the sample from the testing fixture in each step.

The first stage consisted on introducing a pre-crack in the sample by inverse four-point bending test (edge notched subjected to compressive nominal stress) at a load ratio of $R=0.1$. Crack propagation process was carried out under four-point bending test and in this case, crack propagation was conducted by cycling tensile stresses employing R values of 0.1 and 0.5 at 150 Hz approximately.

Stable crack extension was monitored in situ and fatigue crack growth was subsequently determined following a direct-measurement method. Crack growth thresholds, defined at crack growth rates of 10^{-9} m/cycle, were attained following an incremental loading sequence steps. Finally, fatigue sensitivity (δ_f) was calculated in terms of fatigue crack growth threshold and the fracture toughness, according equation (1).

$$\delta_f = 1 - \frac{K_{th}}{K_{Ic}} \quad (1)$$

Several failed specimens were subjected to fractographic examination under scanning electron microscopy (SEM).

2.1.3 Fatigue limit determination

The experimental fatigue limit was performed only for CoMM and CoMC grades. Fatigue limit testing was carried out using rectangular bars of dimensions 45 mm \times 4 mm \times 3 mm. The edges of tested specimens were first slightly chamfered in order to reduce the presence of stress raisers and possible fracture origins. Afterwards, samples were diamond ground and polished to mirror-like finish on the surface which was later subjected to the maximum stress in bending.

Ten samples per grade were tested under four-point bending with inner and outer spans of 20 and 40 mm, respectively. The fatigue limit distribution was determined at 10^6 cycles, following the staircase or up-and-down method, at load ratio of 0.1 and employing a resonant testing machine (working frequencies of about 125Hz). Finally, fatigue sensitivity (δ_f)

was calculated in terms of fatigue limit and the fracture stress, employing equation (2).

$$\delta_f = 1 - \frac{\sigma_f}{\sigma_R} \quad (2)$$

2.3 Metallographic sample preparation for image characterization

2.3.1 Cutting

Characterization of stable crack propagation was carried out using two segments: side face section and orthogonal section to the side face plane. In the case of orthogonal section to the side face plane, sample was cut transversely and afterwards it was ground until overpass the zone of residual stress. Figure 1 illustrates schemes of cut specimens.

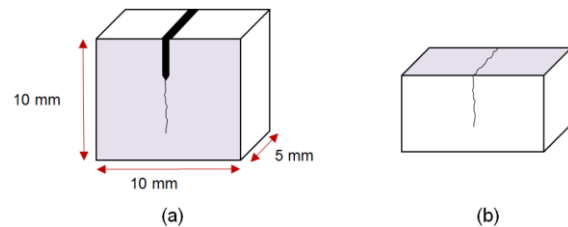


Figure 1: Scheme of samples for image characterization. Shaded segments represent (a) side face section, and (b) orthogonal section to the side face plane (transversal section).

2.3.2 Grinding, polishing and etching

Due to the absence of huge superficial irregularities, a fine grinding process with Magnetic discs MD-System Grinding Discs Struers was suitable enough.

Polishing procedures involved subsequent diamond polishing suspensions, as well as the use of silica colloidal suspension. In addition, an etching process was carried out using Murakami's reagent [15]. This solution was employed at room temperature and it was applied by immersion of the sample.

2.4 Image characterization

The image characterization conducted in this study involved two aspects. Initially, it was assessed from fractographic examination by field emission scanning electron microscopy (FE-SEM) of the failed samples produced by fatigue loading cycles. Additionally, electron backscatter diffraction (EBSD) analysis was conducted for no failed specimens. EBSD evaluation was focused only on CoMC grades because this grade exhibited relative higher mean free path than the other samples. Additionally, a roughness study was carried out by atomic force microscope (AFM), in order to optimize the polishing procedure for EBSD imaging.

2.4.1 Atomic force microscopy analysis

Based on polishing process accomplished in metallographic sample preparation, the surface roughness of five CoMC samples was measured by AFM working in tapping mode. AFM technique was used to evaluate the effect of the colloidal silica polishing between 5 and 30 minutes and the action of Murakami’s solution as etching agent using different etching times.

Testing measurements were carried out in Dimension 3100 Microscope (Bruker). All the images and cross section profiles were processed with the WSxM software [6].

2.4.1 Electron backscatter diffraction analysis.

EBSD studies focused on stable propagated cracks. They were accomplished to characterize crack-microstructure interactions within the cobalt phase. Analysis were carried out on a JEOL 7001F scanning electron microscope equipped with a field emission and an orientation imaging microscopy (OIM) system developed by TSL. Sample was tilted at 70° relative to normal incidence of the electron beam. EBSD measurements were performed with a step size of 0.03 μm, an acceleration voltage of 20 KV, beam currents up to 20 nA and working distance of 10 mm. Automatic analysis software Channel 5 (HKL technology) was used to provide indexing of the crystallographic orientation of the tested sample.

3. RESULTS AND DISCUSSION

3.1 Assessment of fatigue crack growth threshold

FCG threshold (K_{th}) determination involved tracing of the crack growth by optical microscopy. The attained results from fatigue crack growth testing (crack growth per cycle) permitted to obtain the fatigue crack growth threshold. It was calculated based on the trend exhibit by the dependence of crack growth rates as a function of maximum stress intensity factor K_{max} . The corresponding plots for CoMC, CoMM and CoHM grades are presented in Figures 2 and 3.

Paris-Erdogan equation constants as well as fatigue crack growth threshold values are presented in Tables 4 and 5. Considering obtained results, it is evident that K_{th} values are lower than those corresponding to fracture toughness. Additionally, K_{th} values are observed to rise with increasing R.

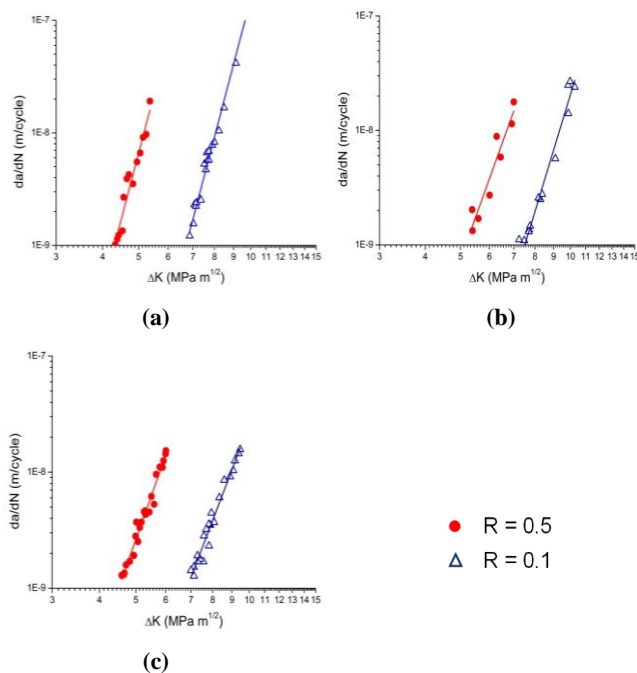


Figure 2: Fatigue crack growth rate as a function of ΔK (a) CoMM, (b) CoMC, and (c) CoHM.

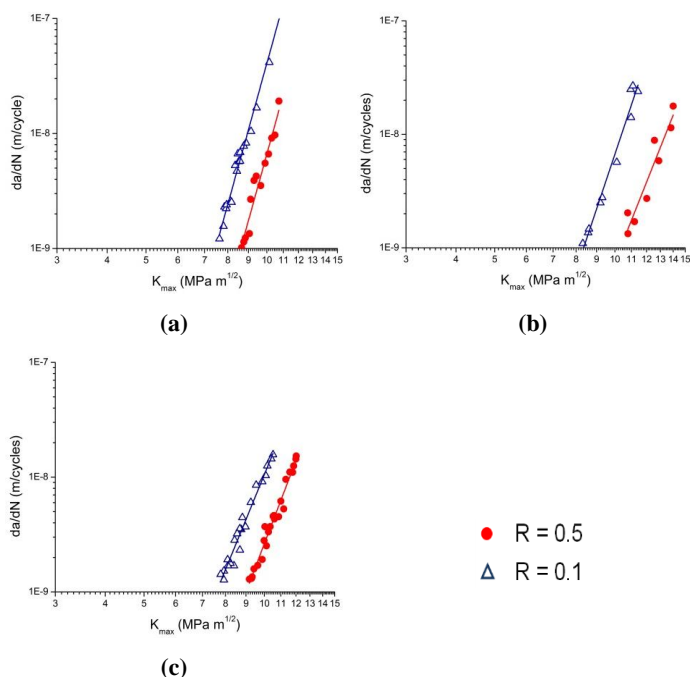


Figure 3: Fatigue crack growth rate as a function of K_{max} (a) CoMM, (b) CoMC, and (c) CoHM.

Table 4: Summary of the experimental fatigue crack growth data at R=0.1

| Grade | C | m | K_{th} (MPa m ^{1/2}) | $1 - \frac{K_{th}}{K_{Ic}}$ |
|-------|------------------------|-------|-------------------------------------|-----------------------------|
| CoMM | 4.62×10^{-20} | 12.40 | 7.50 | 0.47 |
| CoMC | 1.41×10^{-19} | 10.67 | 8.38 | 0.51 |
| CoHM | 2.67×10^{-17} | 8.60 | 7.61 | 0.56 |

Table 5: Summary of the experimental fatigue crack growth data at R=0.5

| Grade | C | m | K_{th} (MPa m ^{1/2}) | $1 - \frac{K_{th}}{K_{Ic}}$ |
|-------|------------------------|------|-------------------------------------|-----------------------------|
| CoMM | 1.06×10^{-20} | 12.6 | 8.60 | 0.39 |
| CoMC | 4.01×10^{-19} | 9.23 | 10.4 | 0.46 |
| CoHM | 1.66×10^{-18} | 9.20 | 9.10 | 0.47 |

Considering CoMM grade as the reference material, the variation in grain size (CoMM→CoMC) and binder content (CoMM→CoHM) led to increase the fatigue crack growth threshold values. In addition, load ratio variation (R=0.1 → R=0.5) produced an intensification of this tendency.

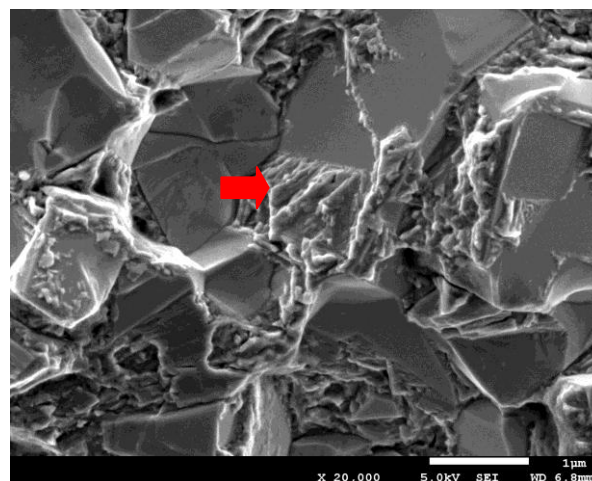
Otherwise, fatigue sensitivity exhibits similar values for the three grades. These results suggest that fatigue sensitivity does not exhibit a significantly dependence of binder content and grain size, at least with the experimental samples here studied. Additionally, in the tested samples the increase load ratio from 0.1 to 0.5 yields lower fatigue sensitivity values

3.1.1 Fatigue crack growth fractography

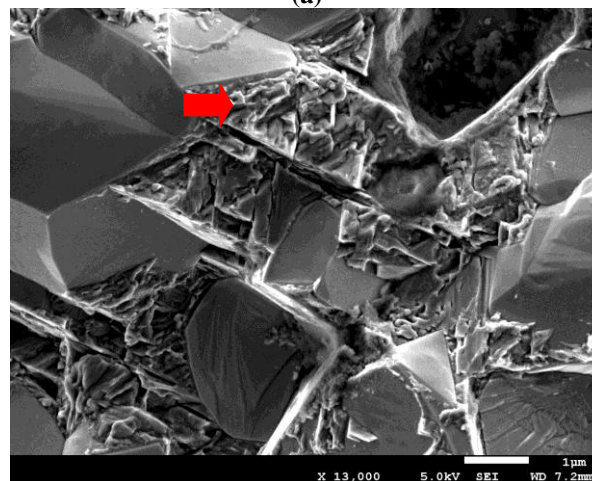
In all cases, the fractography analyses in the flexural strength tests showed surface with agglomerate of coarse grains and abnormally coarse grains as typical fracture initiation sites.

On the other hand, Figure 4 shows deformation micromechanism under fatigue experimented by CoMM and CoMC grades. Regarding cobalt binder phase, fractography image exhibits microstructural evidence of fatigue crack morphologies, which may be describe mainly as “step-like” features (see red arrows). The fatigue crack surfaces of tested samples appear to follow crystallographic planes since steps are nearly parallel. Additionally, it may be consider that fatigue crack growth occurs predominantly by single shear in the direction of primary slip system.

According to Suresh [12] this single step mechanism leading to a “zig-zag” crack path, is known as microscopic stage I of the fatigue crack growth. In agreement with previous works [7], as it may be inferred from these results, premature fracture by fatigue crack growth is produced by the intrinsic fatigue susceptibility of the constrained cobalt binder phase.



(a)



(b)

Figure 4: SEM micrograph showing fractographic features associated with stable crack growth of (a) CoMM grade, and (b) CoMC grade.

3.2 Fatigue limit

The fatigue limit value for the studied hardmetals was assessed taking into account statistical analysis as well as dispersion measurements. After statistical analysis of experimental data obtained by staircase method, mean value for the fatigue limit was determined. Both experimental and observed values together with fatigue sensitivity are presented in Table 6.

Table 6: Fatigue limit data for studied WC-Co hardmetals

| Grade | R=0.1 | | Fatigue Sensitivity $1 - \frac{\sigma_f}{\sigma_R}$ |
|-------|-------------------------------|------------------------------|--|
| | Predicted fatigue limit (MPa) | Observed fatigue limit (MPa) | |
| CoMM | 1629 | 1603 ± 134 | 0.48 |
| CoMC | 1171 | 1246 ± 116 | 0.50 |

The comparison between predicted and observed fatigue limits suggests that there is no significant difference between

their values. Moreover, fatigue sensitivity obtained by staircase methodology is quite similar to those obtained from the ratios determined from FCG threshold and fracture toughness.

In accordance with literature reports [7] [13] [14], the FCG threshold–fatigue limit correlation evaluated within a LEFM framework permits to predict fatigue limit values directly from the ratio K_{th}/K_{Ic} . Such estimation is based on the consideration that the large cracks and small natural flaws exhibit similar FCG behavior as well as the subcritical growth of preexisting defects is the dominant stage of fatigue life behavior. Thus, FCG threshold can be considered as the effective toughness under cycling loading.

3.3 AFM results

AFM analysis conducted in this study has been a strategic tool in order to evaluate sample preparation process. Figure 5 presents 3D-image and a plot of height as a function of width profile for all the samples observed by AFM. Roughness profiles presented in this figure reveal that Murakami’s reagent produces a heterogeneous attack of tungsten carbides. Furthermore, overall AFM results suggest that etching has been produced in preferential areas of tungsten carbides, depending on the crystallographic orientation. As it is reported by Haller [4] the various components of the WC phase microstructure i.e. α -phase: WC, γ -phase: mixed carbides (TiC, TaC, NbC, WC), η -phase: $Co_3W_3C(M_6C)$, $Co_6W_6C(M_{12}C)$ and di-tungsten carbide: W_2C have different reaction rates with Murakami’s reagent because the difference between their crystalline microstructures leading to different hardness values. It has been found that normally α -phase requires longer times than the other phases [1]. Considering this criteria, 8 minutes etching using Murakami’s reagent probably is not enough to obtain flat surfaces. (See S5 in Figure 5(a))

3.3 EBSD results

The phase image Figures 6 and 7 register the presence of both Co-fcc and Co-hcp mainly in the side face section. It must be noticed that their coexistence is not located exclusively near crack trajectory. In addition, indexing data presented in Table 7 exhibits different values of cobalt phases between side face and transversal sections. A possible cause for this behavior may be the stresses generated during machining and/or rough grinding processes.

However, another parameter to take into account is the plastic deformation which could be produced during fatigue crack growth process. Within this context, the extent of near-tip plasticity may influence the cobalt phase transformation (from fcc \rightarrow hcp). Thus, indexed quantity differences observed in present results may also be related with variation of plastic zone between transversal and face side sections.

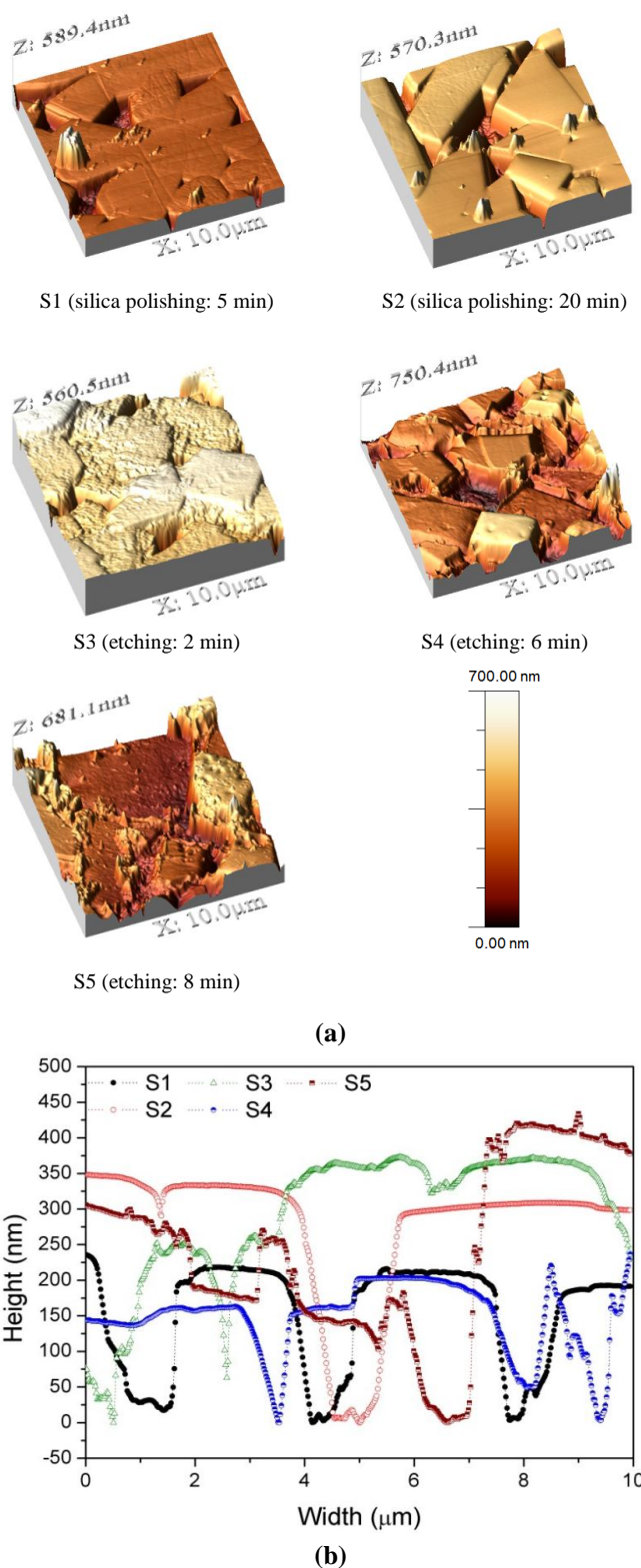


Figure 5: (a) AFM-3D images of roughness analysis (b) AFM topographic surface analysis expressed by roughness profiles.

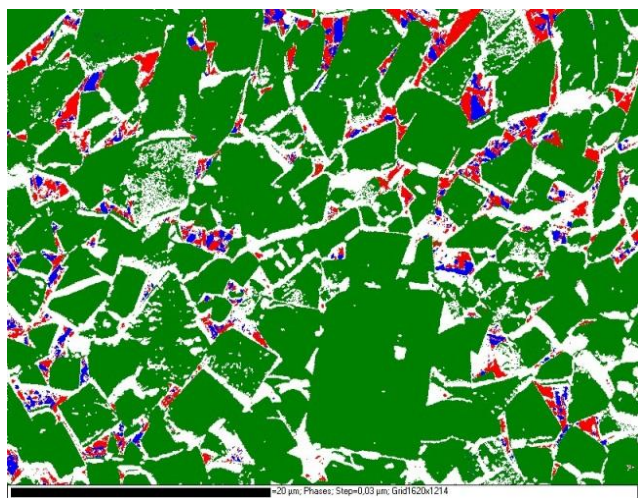


Figure 6: EBSD results of CoMC grade (side face section) showing different phases. Legend: green- WC; red - Co fcc; blue - Co hcp.

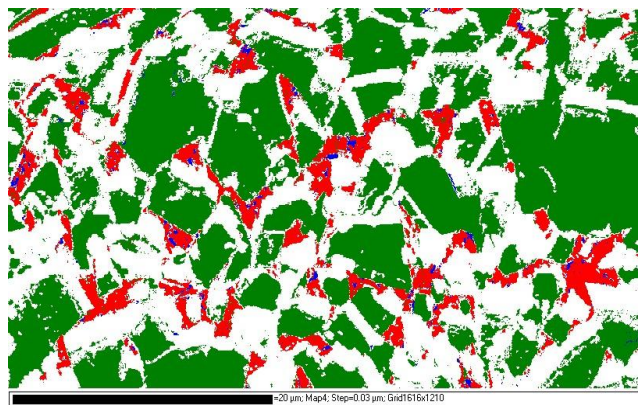


Figure 7: EBSD results of CoMC grade (transversal section) showing different phases. Legend: green- WC; red - Co fcc; blue - Co hcp.

Table 7: EBSD indexing data for CoMC grade.

| Phase | Indexed quantity (%) | |
|--------------|----------------------|---------------------|
| | Side face section | Transversal section |
| WC | 70.2 | 32.9 |
| Cobalt-fcc | 2.55 | 6.23 |
| Cobalt-hcp | 1.42 | 0.50 |
| Non-indexing | 25.8 | 60.4 |

The morphologies observed in fatigue crack fractography (see Figure 4) suggest that the presence of crystallographic planes is related with martensitic transformation within the binder phase. The scarce indexed cobalt-hcp on transversal section and the increase of cobalt-fcc suggest that side faces surfaces of samples experienced fcc→hcp phase transformation. Therefore, as mentioned above it may be deemed that both sections are found in stage I of the fatigue crack growth and consequently plastic zone deformation surrounding the crack tip are confined to distances lower than the mean free path

(λ_{Co}). Nevertheless, the extent of the plastic zone (r_p) in side face section is probably higher than the r_p of the transversal section because there exist a higher stress constriction of the binder in the transversal section.

4. CONCLUSIONS

Analysis of FCG behavior within a fatigue mechanics framework permits to corroborate FCG threshold as the effective fracture toughness under cyclic loading. Attained results confirm that fatigue threshold (K_{th}) values occur at values considerably lower than those of fracture toughness.

Fatigue characteristics of studied samples have been assessed by FCG threshold–fatigue limit correlation. It is found that the FCG threshold-based approach exhibit an excellent concordance between estimated and experimentally determined fatigue limit values. Furthermore, CoMM grade exhibits the lowest fatigue sensitivity, followed by CoMC and CoHM.

FE-SEM fractographic evaluation points out both agglomerate of coarse grains and abnormally coarse grains as critical defects. Additionally, fractographic analyses corroborate that cycling loading fracture surfaces are characterized by “step-like” features which are produced by local plastic deformation of cobalt binder phase.

Effective metallographic sample preparation for EBSD imaging is still a difficult challenge in the assessment of cobalt binder phase in WC-Co hardmetals. In this sense, an appropriated polishing protocol has been defined. However, WC etching process needs to be studied in more detail, with particular emphasis on the etching time influence of Murakami’s reagent.

EBSD results suggest that martensitic transformation of Co binder phase (fcc→hcp) is not exclusively associated with cycling loading, as it had been postulated in the literature. On the other hand, it seems to be induced by rough grinding of the exposed surfaces. From the perspective of fatigue micromechanisms, they are clearly localized within the binder phase, although specific nature (slip/twining) of the crystallographic-like path observed may not be defined at this research stage.

REFERENCES

- [1] ASM International-The Materials Information Society, Tool Materials, J. R. Davis, Ed., p. 501, 1995.
- [2] D. Coureaux, "Comportamiento mecánico de carburos cementados WC-Co: Influencia de la microestructura en la resistencia a la fractura, la sensibilidad a la fatiga y la tolerancia al daño inducido bajo solicitaciones de contacto", Tesis Doctoral, Universitat Politècnica de Catalunya, Barcelona, España, 2012.

[3] G. Erling, S. Kursawe, S. Luyckx and H. G. Sockel, "Stable and unstable fracture surface features in WC-Co," *Journal of Materials Science Letters*, 19 (2000) 437-438.

[4] M. N. Haller, "Metallography and Microstructures of Cemented Carbides," in *Metallography and Microstructures*, vol. 9, ASM Handbook American Society of Metals, pp. 273-278, 1985.

[5] J. Hong and J. Gurland, "A study of the Fracture Process of WC-Co Alloys," in *Science of Hard Materials*, Providence, Springer US, (1983) 649-669.

[6] I. Horcas, J. Fernández, J. Gómez-Rodríguez, J. Colchero, A. Gómez-Herrero and A. Baro, "WSxM software," *Rev. Sci. Instrum.*, 2007.

[7] L. Llanes, Y. Torres and M. Anglada, "On the fatigue crack growth behavior of WC-Co cemented carbides: kinetics description, microstructural effects and fatigue sensitivity," *Acta Materialia*, 50 (2002) 2381-2393.

[8] K. P. Mingard, B. Roebuck, J. Marshall and G. Sweetman, "Some aspects of the structure of cobalt and nickel binder phases in hardmetals," *Acta Materialia*, 59 (2011) 2277-2290

[9] K. P. Mingard, H. G. Jones, M. G. Gee, B. Roebuck and J. W. Nunn, "In situ observation of crack growth in a WC-Co hardmetal and characterisation of crack growth morphologies by EBSD," *International Journal of Refractory Metals and Hard Materials*, 36 (2013) 136-142.

[10] B. Roebuck and E. A. Almond, "Deformation and fracture processes and the physical metallurgy of WC-Co hardmetals," *International Materials Reviews*, 33 (1988) 90-110.

[11] U. Schleinkofer, H.-G. Sockel, K. Gorting and W. Heinrich, "Fatigue of hard metals and cermets," *Materials Science and Engineering: A*, 209 (1996) 313-317.

[12] S. Suresh, *Fatigue of Materials*, Second ed., New York: Cambridge University Press, 2004.

[13] Y. Torres, M. Anglada and L. Llanes, "Fatigue mechanics of WC-Co cemented carbides," *International Journal of Refractory Metals and Hard Materials*, 19 (2001) 341-348

[14] Y. Torres, S. Rodríguez, A. Mateo, M. Anglada and L. Llanes, "Fatigue behavior of powder metallurgy high-speed steels: fatigue limit prediction using a crack growth threshold-based approach," *Materials Science and Engineering: A*, 387-389 (2004) 501-504

[15] G. Vander Voort, *Metallography, principles and practice*, Ohio: ASTM International, 2004